

## Superfluid $^3\text{He}$ in very confined regular geometries

Ying-Hong Li and Tin-Lun Ho

*Department of Physics, Ohio State University, Columbus, Ohio 43210*

(Received 20 October 1987)

Superfluid  $^3\text{He}$  in very narrow slab and cylindrical geometries is studied using the Ginzburg-Landau approach. It is found that, in the case of very narrow slabs, the effect of the boundary is to favor the formation of the  $A$  phase. At lower temperatures, this  $A$  phase is unstable against a deformed  $B$  phase. Both states are locally stable and can be supercooled or superheated. The phase diagram for  $^3\text{He}$  in a narrow slab resembles that of  $^3\text{He}$  in a magnetic field. The superfluid densities along the channel for both diffusive and specular boundary conditions are computed. Similar results are obtained for a cylindrical geometry. In addition, we present an analytic scheme for determining the order parameter in other geometries in the "very strongly confined" limit.

### I. INTRODUCTION

While there is great understanding of the bulk properties of  $^3\text{He}$  superfluids,<sup>1</sup> comparable understanding has not been achieved for  $^3\text{He}$  in confined geometries.

Confined geometries are usually used to increase the magnitudes of critical currents in flow experiments. The geometries commonly used (such as those made of Vycor glass or packed powder) have a high degree of porosity and contain a large number of small channels. These small channels act as pinning sites of the order parameter. The depairing effects of the channel surfaces also change the order parameter from its bulk form. The deformation of the order parameter increases as the channel size decreases. Such deformations imply the possibility of producing "new" superfluids, which has gradually become a strong motivation for using confined geometries.

Experimentally, increasingly many pronounced effects are found for  $^3\text{He}$  in confined geometries. For example, the phase boundary of the vortex core transition of bulk  $^3\text{He}$  is altered significantly when the transition takes place in small channels.<sup>2</sup> Recently, a novel dissipation mechanism is found in both rotating  $A$  and  $B$  phases.<sup>3</sup> The dissipation in the fluid increases quadratically as the rotational frequency. This dissipation phenomenon also seems to have an analog in heavy-fermion superconductors.<sup>4</sup>

However, the irregular geometries used in many experiments make theoretical studies of the superfluid properties formidable. Very recently, however, experiments<sup>5</sup> have been done in cells consisting of very narrowly spaced ( $\sim 2500$  Å) parallel plates. It is observed that in such geometries, the bulk  $B$  phase turns into the  $A$  phase. The purpose of this paper is to study the structure of  $^3\text{He}$  superfluids in regular geometries such as slabs and cylindrical channels in the "strongly confined limit" (defined later). Using the Ginzburg-Landau theory, we find that independent of the nature of surface scattering (diffusive or specular), the effect of the surface is to favor the formation of  $A$ -like phases: pure  $A$  phase for slabs, and the

" $A$ -polar" phase for cylinders. Although these states become unstable to a deformed  $B$  phase at lower temperatures, they are locally stable and can be supercooled. The phase diagram of  $^3\text{He}$  in these geometries in the strongly confined limit resembles that of  $^3\text{He}$  in a magnetic field.

By confined geometries, we refer to containers with size  $D$  less than the dipolar length  $L_{\text{dipole}} \sim 12$   $\mu\text{m}$ . On these length scales, the dipole energy is small compared to the bending energy of the order parameter. It serves merely as a perturbation to fix the degeneracy of the spin degree of freedom. In what follows, we shall consider the case  $L_{\text{dipole}} > D \gg \xi_0$ , where  $\xi_0$  is the zero temperature coherence length. [According to Ref. 6,  $\xi_0$  varies significantly with pressure  $P$ . It varies from 89.4 to 404 Å as  $P$  changes from 34.2 to 0 bar.] For containers of such dimensions, the Ginzburg-Landau description is applicable near  $T_c$ .

In addition to this "confined condition,"  $L_{\text{dipole}} > D \gg \xi_0$ , it is useful to distinguish the following two cases: (i)  $D \gg \xi(T)$  and (ii)  $D \sim \xi(T)$ , referred to as "mildly" and "strongly" confined limits, respectively. The quantity  $\xi(T) \equiv \xi_0 / (1 - T/T_c)^{1/2}$  is the temperature-dependent coherence length. In the mildly confined limit, (i), the order parameter is slightly deformed from its bulk form. The effect of the confined geometry is to pin the orbital part of the order parameter. In the strongly confined limit, (ii), the order parameter differs significantly from its bulk structure. Since  $\xi(T)$  increases as  $T$  approaches to  $T_c$ , one can always reach the strongly confined limit by getting sufficiently close to  $T_c$ . For container size  $D \sim \mu\text{m}$ , condition (ii) implies  $(1 - T/T_c) \sim (\xi_0/D)^2$ , which is a very small temperature range about  $10^{-2}$  mK for all pressures. However, when  $D$  is about 2500 Å, the strongly confined temperature range becomes much wider, about 1 mK (see also Figs. 1–3 below). Most of the recent experiments such as those in Refs. 2 and 4 were done in the mildly confined limit. The experiment in Ref. 5, however, was done in the strongly confined limit.

The Ginzburg-Landau functional<sup>1</sup> of  $^3\text{He}$  as a function of the order parameter  $A_{\mu i}$  is  $\int F = \int (F_B + F_G)$ ,

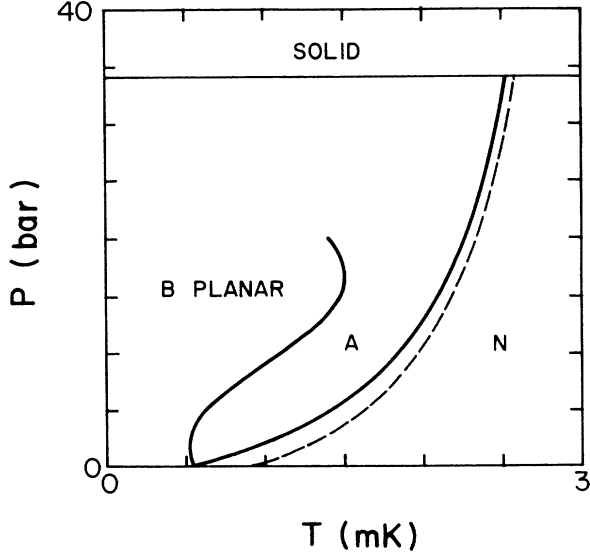


FIG. 1. The phase diagram of  $^3\text{He}$  in slab geometry for  $D=2000 \text{ \AA}$  and diffusive boundary condition. The dashed line is the super-to-normal fluid phase boundary of the bulk  $^3\text{He}$  ( $D=\infty$ ).

$$F_B = -\alpha A_{\mu i} A_{\mu i}^* + \beta_1 A_{\mu j} A_{\mu j} A_{\nu i}^* A_{\nu i}^* + \beta_2 A_{\mu i} A_{\mu i}^* A_{\nu j} A_{\nu j}^* + \beta_3 A_{\mu j} A_{\nu j} A_{\nu i}^* A_{\mu i}^* + \beta_4 A_{\mu j} A_{\nu j}^* A_{\nu i} A_{\mu i}^* + \beta_5 A_{\mu j} A_{\nu j}^* A_{\nu i}^* A_{\mu i}, \quad (1)$$

$$F_G = K[(\gamma - 1)\nabla_j A_{\mu j} \nabla_i A_{\mu i}^* + \nabla_j A_{\mu i} \nabla_j A_{\mu i}^*], \quad (2)$$

where

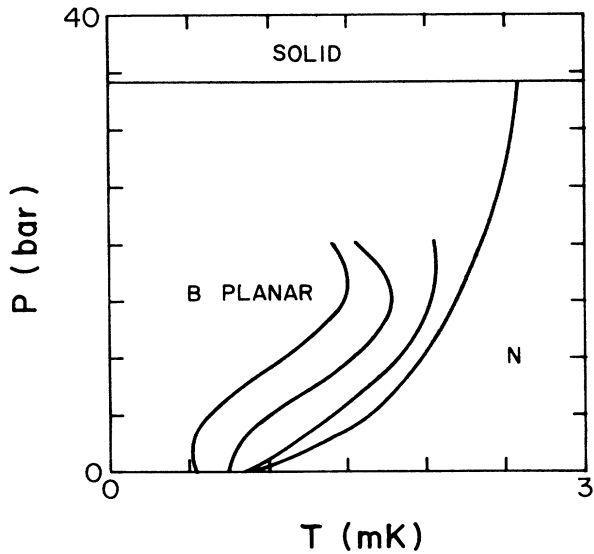


FIG. 2. The phase boundary between the  $A$  and  $B$ -planar phase as a function of plate spacing  $D$ . Diffusive boundary condition. The four boundaries from left to right correspond to  $D=2000, 3000, \text{ and } 5000 \text{ \AA}$ , and  $\infty$ .

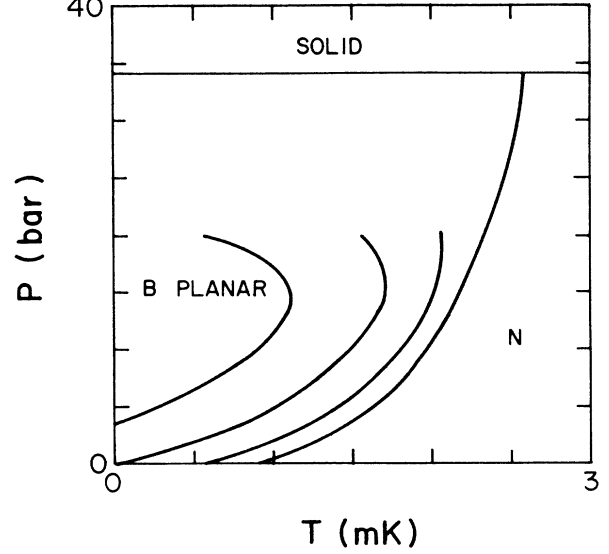


FIG. 3. Same as Fig. 2 except for specular boundary condition.

$$\alpha = \alpha(T) = N(0)(1 - T/T_c)/3,$$

$$K = \frac{7\zeta(3)}{240} N(0) \left[ \frac{\hbar v_F}{\pi k_B T_c} \right]^2$$

$$\equiv \alpha(T) \xi^2(T)$$

$$\equiv \alpha(T) \xi_0^2 (1 - T/T_c),$$

$$\gamma = 3.$$

For the present discussions, it is useful to use a scaled order parameter  $a_{\mu i} = A_{\mu i}/\Delta_B$  and a scaled gradient  $\partial = \xi(T)\nabla$ , where  $\Delta_B = [\alpha/2(3\beta_{12} + \beta_{345})]^{1/2}$  is the equilibrium  $B$ -phase order parameter in the bulk. Here, we used the notation  $\beta_{12} \equiv \beta_1 + \beta_2$  and  $\beta_{345} \equiv \beta_3 + \beta_4 + \beta_5$ , etc. Defining  $f = F/(\alpha(T)\Delta_B^2)$ , the free energy can now be written in a dimensionless form  $\int f = \int (f_B + f_G)$ ,

$$f_B = -a_{\mu i} a_{\mu i}^* + \frac{1}{2} \zeta_1 a_{\mu j} a_{\mu j} a_{\nu i}^* a_{\nu i}^* + \frac{1}{2} \zeta_2 a_{\mu i} a_{\mu i}^* a_{\nu j} a_{\nu j}^* + \frac{1}{2} \zeta_3 a_{\mu j} a_{\nu j} a_{\nu i}^* a_{\mu i}^* + \frac{1}{2} \zeta_4 a_{\mu j} a_{\nu j}^* a_{\nu i} a_{\mu i}^* + \frac{1}{2} \zeta_5 a_{\mu j} a_{\nu j}^* a_{\nu i}^* a_{\mu i}, \quad (3)$$

$$f_G = (\gamma - 1) \partial_j a_{\mu j} \partial_i a_{\mu i}^* + \partial_j a_{\mu i} \partial_j a_{\mu i}^*, \quad (4)$$

where  $\zeta_j = \beta_j/(3\beta_{12} + \beta_{345})$ .

The equilibrium states are determined by the stationary condition

$$0 = \frac{\delta f}{\delta a_{\mu i}^*} = -a_{\mu i} + \zeta_1 a_{\nu j} a_{\nu j} a_{\mu i}^* + \zeta_2 a_{\nu j} a_{\nu j}^* a_{\mu i} + \zeta_3 a_{\mu j} a_{\nu j} a_{\nu i}^* + \zeta_4 a_{\mu j} a_{\nu j}^* a_{\nu i} + \zeta_5 a_{\nu i} a_{\nu j} a_{\mu j}^* - (\gamma - 1) \partial_i \partial_j a_{\mu j} - \partial_j \partial_j a_{\mu i} \quad (5)$$

and the boundary condition at the surface. Depending on whether the surface scattering is diffusive or specular, the boundary condition<sup>7</sup> is  $a_{\mu i} = 0$  (diffusive scattering) or  $a_{\mu i} \hat{n}_i = 0$ ,  $a_{\mu i} \hat{m}_i \neq 0$  (specular scattering), where  $\hat{n}$  and  $\hat{m}$  are directions normal and parallel to the surface, respectively.

## II. SLAB GEOMETRY

We shall first summarize our results. Let  $\hat{z}$  be the direction normal to the plates with separation  $D$ . We have found that in the strongly confined limit, for both specular and diffusive surface scattering, there are only two stable states, of the forms

$$A_{\mu i}(z) = v(z) \hat{z}_\mu (\hat{x} + i \hat{y})_i, \quad (6)$$

$$A_{\mu i}(z) = h(z) \hat{z}_\mu \hat{z}_i + g(z) (\hat{x}_\mu \hat{x}_i + \hat{y}_\mu \hat{y}_i), \quad (7)$$

referred to as pure  $A$  and  $B$ -planar phase, respectively.

(i) Diffusive scattering. The  $A$  phase is lower in energy than the  $B$ -planar phase when the dimensionless spacing  $D/\xi(T)$  is less than a critical value which increases monotonically with pressure (for example, when  $P=4$  bars, this critical value is 6.5). The phase boundary separating these two phases is shown in Fig. 1 for  $D=2000$  Å. The variation of this phase boundary as  $D$  changes is shown in Fig. 2. The phase boundaries between the  $A$  phase and the normal fluid for different  $D$  are all very close to original bulk phase boundary and are not shown here. These boundaries are represented by  $D/\xi(T) = \pi$ , or  $T(P) = T_c(P)[1 - (\pi\xi_0(P)/D)^2]$ .

(ii) Specular scattering. Again, the  $A$  phase is lower in energy than the  $B$ -planar phase when the ratio  $D/\xi(T)$  is less than a critical value which increases monotonically with pressure. This critical value is larger than that in the diffusive case at the same pressure. For  $P=0$  bars, this critical value is 7.5. The phase boundary separating these two phases for different  $D$  is shown in Fig. 3. The boundary separating the  $A$  phase and the normal fluid is identical to the original bulk phase boundary for all  $D$ .

It is clear from Figs. 1–3 that the phase boundary between the  $A$  and  $B$  phases are quite far away from  $T_c$  at higher pressures. At those pressures, the Ginzburg-Landau theory will not be accurate. Nevertheless, the Ginzburg-Landau phase diagrams still give a qualitative picture for the regions where the  $A$  phase is stable.

The above conclusions are obtained both numerically and analytically. We have found numerically no other stable states than these two. The details of our numerical procedure is presented in Appendix A. In Appendix B, we prove that these two states are indeed locally stable (the local stability can also be checked numerically).

We have also calculated the superfluid density  $\rho_s^{yy}$  along the channel for both specular and diffusive surfaces. The results are summarized in Fig. 4. The calculation of superfluid densities in confined geometries turns out to be quite subtle, as pointed out to us by Thuneberg. The point is that in confined geometries, the order parameter may be very sensitive to external flows. A small flow  $u$  can cause a first-order change ( $\sim u$ ) in the order parameter, which may contribute substantially to  $\rho_s$ . We

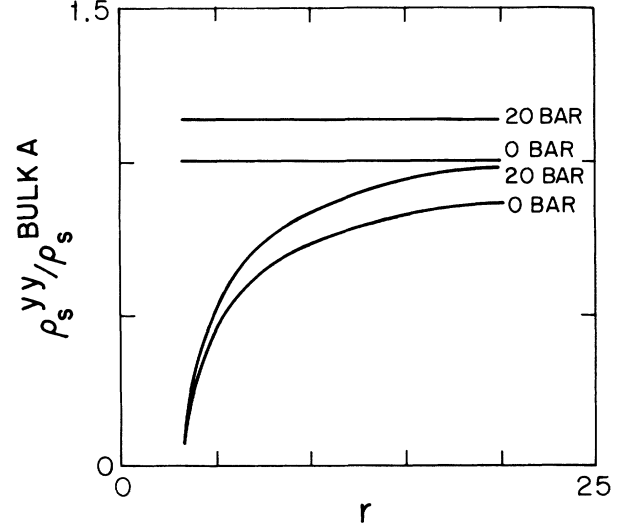


FIG. 4. Superfluid density  $\rho_s^{yy}/\rho_s^{\text{bulk } A}$  along the channel at 0 and 20 bars, where  $\rho_s^{\text{bulk } A} = [5\alpha/(3\beta_{12} + \beta_{345})](2m/\hbar)^2$ .  $d \equiv D/\xi(T)$  is the dimensionless spacing between two parallel plates. The straight and curved lines corresponds to specular and diffusive boundary conditions, respectively.

shall describe this calculation and effects of external superflows in Appendix C.

That we have only found the two states [Eqs. (6) and (7)] in the case of zero external flow appears to be at variance with a recent study of Thuneberg<sup>8</sup> on the depairing effect of a semi-infinite planar surface. Thuneberg found a stable surface state which is very much  $A$ -like, but not exactly a pure- $A$  structure. Since the non- $A$  components of his state is only appreciable near the surface, it seems that their existence is favored by the surface and should therefore be present in the slab geometry. We have not, however, found a stable state of such character. Nor have we understood the reason for the absence of the slab analog of such structure.

The states of the lowest energy within the families (6) and (7) are specified by real amplitudes  $v_0$ ,  $h_0$ , and  $g_0$ , which satisfy the stationary conditions within each family,

$$v'' + v - 2\zeta_{245}v^3 = 0, \quad (8)$$

$$\gamma h'' + h - \zeta_{12}(h^2 + 2g^2)h - \zeta_{345}h^3 = 0, \quad (9)$$

$$g'' + g - \zeta_{12}(h^2 + 2g^2)g - \zeta_{345}g^3 = 0, \quad (10)$$

for pure  $A$ ,  $B$ -planar, and  $B$ -planar, respectively, where  $\zeta_{245} \equiv \zeta_2 + \zeta_4 + \zeta_5$ . Solutions  $v_0$ ,  $g_0$ , and  $h_0$  are shown in Fig. 5. It is straightforward to show that these lowest-energy states are also stationary points in the entire order parameter space, i.e., they are solutions of Eq. (5).

In the case of the  $B$ -planar family, Eq. (7),  $g_0$  is always greater than  $h_0$  for both diffusive and specular boundary condition. In particular, for thick slabs, and with diffusive boundary condition,  $h_0$  has a shoulder near the surface larger in magnitude than that of the bulk order

parameter (see Fig. 5). For thin slabs, both  $g_0$  and  $h_0$  approach the sine function (see discussions below).

The phase boundaries between  $A$  and  $B$ -planar shown in Figs. 1, and 2, and 3 are obtained by equating free energies associated with (6) and (7),

$$f_A(v_0, \xi(T)/D) = f_{B\text{-planar}}(h_0, g_0, \xi(T)/D), \quad (11)$$

where [with  $d \equiv D/\xi(T)$ ]

$$f_A(v) = \int_0^d dz (-2v^2 + 2\zeta_{245}v^4 + 2v'^2), \quad (12)$$

$$f_{B\text{-planar}}(h, g) = \int_0^d dz [-(h^2 + g^2) + \frac{1}{2}\zeta_{12}(h^2 + 2g^2)^2 + \frac{1}{2}\zeta_{345}(h^4 + g^4) + \gamma h'^2 + 2g'^2]. \quad (13)$$

The pressure dependence of the free energy enters through the  $\beta$  coefficients and  $\xi_0$ . The  $\beta$  coefficients we used are the ones calculated by Bedell and Pfitzner.<sup>9</sup> The zero-temperature coherence length  $\xi_0$  the Bardeen-Cooper-Schrieffer (BCS) value, which is tabulated in Ref. 6.

We end this section by pointing out another way to understand the structure of the order parameter in the "very" strongly confined limit. The method is generalizable to other geometries. It also shows how the  $A$  to normal fluid phase boundary is determined. To illustrate the method, let us consider the case of diffusive boundary condition. For slab geometry, one can expand the order parameter as

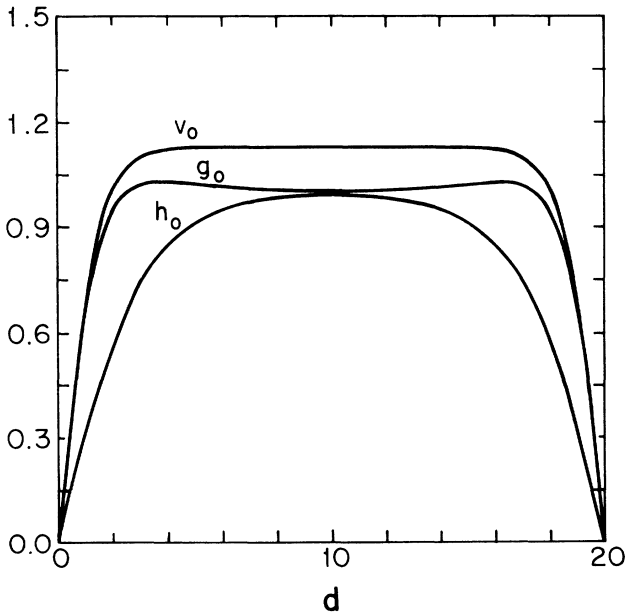


FIG. 5. Spatial dependences of the order parameters of the  $A$  phase ( $v_0$ ) and the deformed  $B$  phase ( $g_0, h_0$ ) in slab geometries for dimensionless spacing  $d \equiv D/\xi(T) = 20$  and pressure  $P = 4$  bars. All order parameters are normalized such that the magnitude of the order parameter of the bulk  $B$  phase is unity.

$$a_{\mu i} = \sum_{n=1}^{\infty} a_{\mu i}^{(n)} \sin(n\pi z/d). \quad (14)$$

The free energy of Eq. (3) plus Eq. (4) can be expressed in terms of the various "components"  $a^{(n)}$  and is of the form

$$f = \sum_{n=1}^{\infty} \left\{ -\frac{1}{2} [1 - \gamma(n\pi/d)^2] |a_{\mu z}^{(n)}|^2 - \frac{1}{2} [1 - (n\pi/d)^2] (|a_{\mu x}^{(n)}|^2 + |a_{\mu y}^{(n)}|^2) + F^{(4)}(a^{(n)}) \right\} + G, \quad (15)$$

where  $F^{(4)}(a^{(n)})$  is the fourth-order term in bulk free energy with order parameter  $a^{(n)}$ , and  $G$  is the coupling between different components  $a^{(n)}$  and  $a^{(m)}$ ,  $n \neq m$ . The effect of the boundary is to give different components a different second-order coefficients.

If the second-order coefficient of a component is positive, this component will be absent in equilibrium unless it is coupled to other components (which have negative second-order coefficients) through  $G$ . As the system approaches the very confined limit [i.e.,  $d = D/\xi(T)$  keeps decreasing], it reaches a point when all the second-order coefficients except those associated with  $a_{\mu x}^{(1)}$  and  $a_{\mu y}^{(1)}$  are positive. In this case, it is sufficient to keep only these two components in Eq. (15) and to consider all other components as perturbations. The problem of minimizing Eq. (4) in the very strongly confined limit reduces to the simple problem of minimizing a bulk free energy for the class of order parameters with only two components,  $a_{\mu x}^{(1)}$  and  $a_{\mu y}^{(1)}$ , and the superfluid can be viewed as two dimensional. With the  $\zeta$ 's tabulated in Table I, it is straightforward to show that the pure  $A$  phase is indeed the state of lowest energy near  $T_c$ . It is easy to see from Eq. (15) that the phase boundary between the  $A$  phase and the normal fluid is given by  $D/\xi(T) \equiv d = \pi$ , or  $T = T_c(P) \{1 - [\pi\xi_0(P)/D]^2\}$ . Following the same procedure, it is also easy to show that for specular surfaces, the  $A$ -to-normal phase boundary for all  $D$  is identical to that of the bulk superfluid (i.e.,  $D = \infty$ ).

For other geometries, the analogous set of orthogonal functions defined by the geometry and boundary condi-

TABLE I. Table of the  $\zeta$  coefficients.  $\zeta_j \equiv \beta_j / (3\beta_{12} + \beta_{345})$ .

$P$ (bar)	$\zeta_1$	$\zeta_2$	$\zeta_3$	$\zeta_4$	$\zeta_5$
0	$-\frac{1}{5}$	$\frac{2}{5}$	$\frac{2}{5}$	$\frac{2}{5}$	$-\frac{2}{5}$
4	-0.214	0.418	0.416	0.410	-0.438
8	-0.231	0.439	0.434	0.422	-0.481
12	-0.249	0.463	0.454	0.434	-0.529
16	-0.259	0.476	0.466	0.441	-0.556
20	-0.268	0.488	0.477	0.447	-0.583
24	-0.278	0.500	0.490	0.455	-0.611
28	-0.286	0.511	0.501	0.461	-0.638

tion. Referring the (matrix) coefficients of the different orthogonal functions as different superfluid components, it is easy to see that the Ginzburg-Landau free energy in the very confined limit can always be reduced to the bulk free energy of a one- or two-components superfluids.

III. CYLINDRICAL CHANNELS

The case of cylindrical channel has been studied by Fishmann and Privorotskii,<sup>10</sup> and by Muzikar.<sup>11</sup> These authors noted that for sufficiently small channels, the most favorable state is the one with a polar core. We have calculated the phase diagram of a class of axisymmetric states (defined below) which we believe to be the ones of lowest energy. When going from the strongly confined to the mildly confined limit, the system makes a transition from an *A* polar state to a *B*-like state.

Again, we first summarize our results. Let  $\hat{z}$  be the symmetry axis of a cylindrical channel of radius *R*. The class of states we consider are of the form  $A_{\mu i}(r, \phi) = D_{\nu j} \hat{e}_{\mu}^{(\nu)} \hat{e}_i^{(j)}$ , where  $(\hat{e}^{(1)}, \hat{e}^{(2)}, \hat{e}^{(3)}) = (\hat{r}, \hat{\phi}, \hat{z})$ , and  $D_{\mu i}$  depends only on *r*. In the very confined regime, we have found two stable states, referred to as *A*-polar and deformed *B*, respectively:

$$A_{\mu i}(r, \phi) = \hat{z}_{\mu} [D_3(r) \hat{z}_i + iD_1(r) \hat{r}_i + iD_2 \hat{\phi}_i], \quad (16)$$

$$A_{\mu i}(r, \phi) = D_3 \hat{z}_{\mu} \hat{z}_i + D_1(r) \hat{r}_{\mu} \hat{r}_i + D_2(r) \hat{\phi}_{\mu} \hat{\phi}_i. \quad (17)$$

These states are shown in Fig. 6. The phase boundaries between these two states for diffusive and specular boundary conditions are shown in Figs. 7 and 8, respectively.

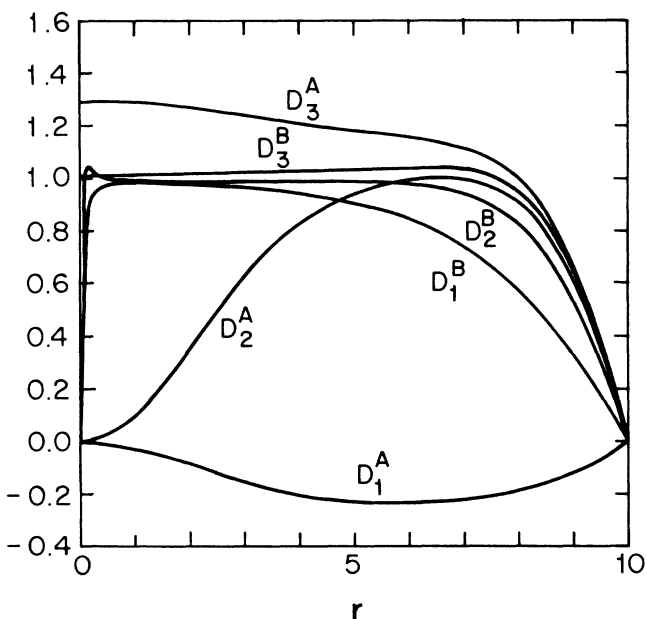


FIG. 6. Spatial dependence of the order parameters of the *A*-polar phase ( $D_i^A$ 's) and the deformed *B* phase ( $D_i^B$ 's) in cylindrical geometries with the same dimensionless radius  $r \equiv R/\xi(T) = 10$  and pressure  $P = 4$  bars. The normalization of the order parameters is identical to that in Fig. 5.

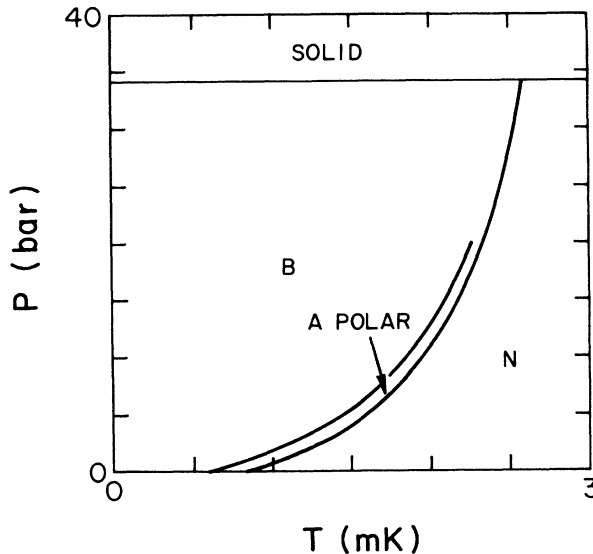


FIG. 7. The phase diagram of <sup>3</sup>He in a cylinder of radius  $R = 3000 \text{ \AA}$  for diffusive boundary condition.

tively. The phase boundary separating the *A*-polar phase and the normal fluid for diffusive surface scattering is given by

$$T(P) = T_c(P) \{ 1 - [\xi_0(P)/R]^2 (1 + \pi^2/4) / (1 - 4/\pi^2) \}. \quad (18)$$

For specular scattering, this phase boundary is identical to that of the bulk, i.e.,  $T(P) = T_c(P)$ . The corresponding superfluid densities along the channel are shown in Fig. 9. The local stability of (16) has been proved in Ref. 10. The

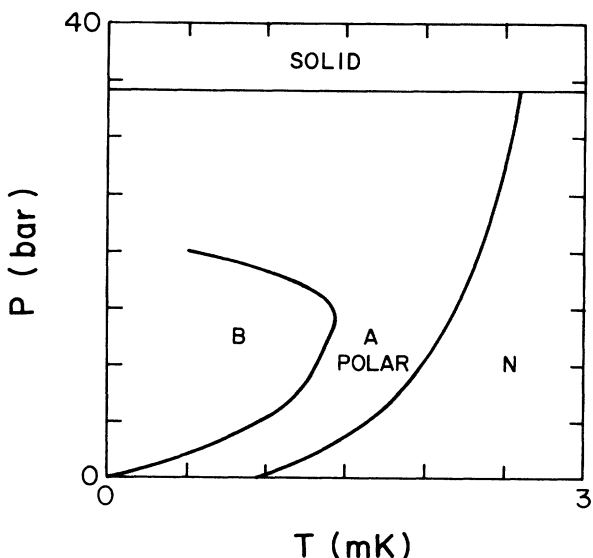


FIG. 8. The phase diagram of <sup>3</sup>He in a cylinder of radius  $R = 3000 \text{ \AA}$  for specular boundary condition.

local stability of (17) can be shown similarly and will not be presented here. These local stabilities can also be tested easily by numerical methods.

It should be noted that unlike the slab geometry, the phase diagrams (Figs. 6 and 7) for small cylinders with diffusive and specular surface scattering are very different. In the case of diffusive surface scattering, the  $A$ -polar state is stabilized only within a narrow range near  $T_c$  below the polycritical point. In the specular case, this range is much wider. The reason is simply that for both specular and diffusive surfaces, the dominant part of the order parameter in cylinders with small radii is the polar component  $\hat{z}_\mu \hat{z}_i$  (which is also the surviving component when  $T$  is very close to  $T_c$ ). In the specular case, this polar component is fairly constant throughout the channel even for small radii. On the other hand, in the diffusive case, this polar state will be strongly suppressed. The systems no longer can take advantage of the condensation energy coming from this last remaining state.

Our conclusions are derived as follows. In terms of  $D_{\mu i}$ , the bulk free energy  $f_B$  is given by (1) with the  $\mathbf{a}$ 's replaced by  $\mathbf{D}$ 's. The gradient energy  $f_G$ , however, becomes

$$\begin{aligned}
 f_G = \sum_{\mu} ( & |\partial_r D_{\mu r}|^2 + |\partial_r D_{\mu \phi}|^2 + |\partial_r D_{\mu z}|^2 ) + ( |\partial_\phi D_{zz}|^2 + |\partial_\phi D_{\phi z} + D_{rz}|^2 + |\partial_\phi D_{rr} - D_{\phi r} - D_{r\phi}|^2 \\
 & + |\partial_\phi D_{\phi r} + D_{rr} - D_{\phi\phi}|^2 + |\partial_\phi D_{zr} - D_{z\phi}|^2 \\
 & + |\partial_\phi D_{r\phi} - D_{\phi\phi} + D_{rr}|^2 + |\partial_\phi D_{\phi\phi} + D_{r\phi} + D_{\phi r}|^2 \\
 & + |\partial_\phi D_{z\phi} + D_{zr}|^2 ) / r^2 \\
 & + (\gamma - 1) |\partial_r D_{rr} + (\partial_\phi D_{rr} - D_{\phi\phi} + D_{rr}) / r^2| + (\gamma - 1) |\partial_r D_{\phi r} + (\partial_\phi D_{\phi\phi} + D_{r\phi} + D_{\phi r}) / r|^2 \\
 & + (\gamma - 1) |\partial_r D_{zr} + (\partial_\phi D_{z\phi} + D_{zr}) / r|^2 .
 \end{aligned} \tag{19}$$

Considering the class of states such that  $D_{\mu i} \equiv D_{\mu i}(r)$ , it is straightforward to use the numerical method discussed in Appendix A to find stationary states. The phase boundaries are calculated in exactly the same way as in the slab geometry. To determine the  $A$ -polar to normal fluid phase boundary, we follow the same procedure as in the case of slab geometry. For diffusive scattering, we can expand the axisymmetric  $D$ 's in a Fourier series

$$D_{\mu i} = \sum_{n=1}^{\infty} [d^{(n)} \cos(n\pi r / 2\rho) + c^{(n)} \sin(n\pi r / 2\rho)]_{\mu i} ,$$

where  $\rho \equiv R / \xi(T)$ . It is easy to see that near  $T_c$ , the component with smallest second-order coefficient is  $d_{zz}^{(1)}$ . The corresponding second-order term reads

$$\int_0^\rho [ -\cos^2(\pi r / 2\rho) + (\pi / 2\rho)^2 \sin^2(\pi r / 2\rho) ] r dr d_{zz}^2 = \frac{d_{zz}^2}{4} \left[ \left[ -\frac{\pi^2}{4} + 1 \right] (2\rho / \pi)^2 + \left[ \frac{\pi^2}{4} + 1 \right] \right] ,$$

which vanishes when  $(2\rho / \pi)^2 = [(\pi^2 / 4) + 1] / [(\pi^2 / 4) - 1]$ , or equivalently, Eq. (18). Similar procedure for the case of specular scattering shows that the  $A$ -polar-to-normal phase boundary is identical to that of the bulk.

#### ACKNOWLEDGMENTS

This work was started during a visit to Cornell University. We would like to thank M. Freeman and R. C.

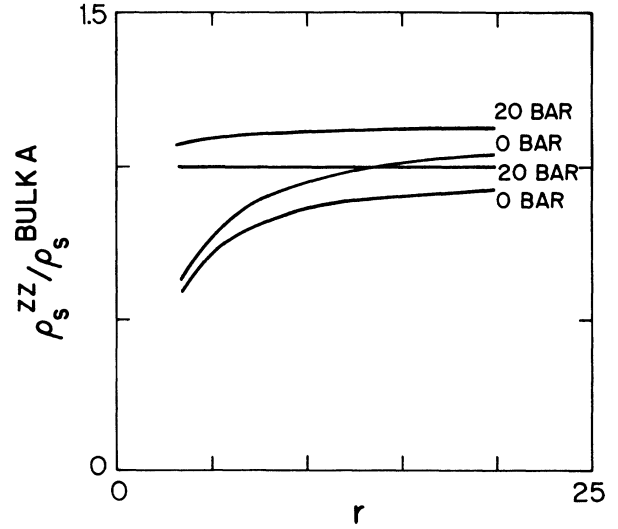


FIG. 9. Superfluid density  $\rho_s^{zz} / \rho_s^{\text{bulk}}$  along a cylindrical channel at 0 and 20 bars. The almost flat curves are for specular boundary condition; and the other two are for diffusive boundary condition.  $r \equiv R / \xi(T)$  is the dimensionless radius of the cylinder.

Richardson for discussions of their fascinating experiments, and E. Thuneberg for pointing out to us the subtle point discussed in Appendix C. While this work was being completed, one of us (T.L.H.) learned in the 1987

workshop at the Aspen Center for Physics that A. L. Fetter and co-workers have studied the same problem and reached the same conclusions. We would like to thank him for discussions. This work was supported in part by the Alfred P. Sloan Foundation and by the National Science Foundation under Grant No. DMR-8717574 for one of us (T.L.H.) and by the National Science Foundation under Grant No. DMR86-13368.

#### APPENDIX A: THE NUMERICAL SOLUTION OF THE STATIONARY EQUATION (5)

In solving Eq. (5), we have used relaxation method<sup>12,13</sup> and the mesh changing method. In the relaxation method, one introduces a lattice in the region of interest, and then iterates the matrix equation

$$a_{\mu i}(n+1; \mathbf{r}) = a_{\mu i}(n; \mathbf{r}) - c \frac{\delta f}{\delta a_{\mu i}^*} \quad (\text{A1})$$

until it converges. Here,  $n$  is an integer labeling the generation of iteration,  $\mathbf{r}$  is a lattice site, and  $c$  (the range we used is 0.8 to 0.001) is a positive constant to be adjusted

to optimize the convergence rate. Equation (20) is essentially a time-dependent Landau-Ginzburg equation with time discretized in constant steps. It has been shown in Ref. 13 that the free energy monotonically decreases as  $n$  increases. The order parameter always relaxes to a local minimum if a sufficiently small  $c$  is used in the iteration.<sup>13</sup> A mesh changing method can be further used to accelerate the converging process: First, one solves Eq. (A1) on a mesh with few points, where the convergence can be achieved quickly. One then introduces additional points to create a denser mesh, and restarts the iteration using the solution obtained from the previous step as new trial function.

#### APPENDIX B: PROOF OF LOCAL STABILITIES OF EQUATIONS (6) and (7)

Let  $a_0$  be a solution of the stationary condition Eq. (5). This is locally stable if the energy change  $Q$  caused by any small deviation  $\epsilon$  from  $a_0$  is positive. The energy change is of the form

$$Q \equiv \frac{1}{2} \frac{\delta^2 F}{\delta a_{\mu i} \delta a_{\nu j}} \bigg|_{a_0} \epsilon_{\mu i} \epsilon_{\nu j} + \text{c.c.} + \frac{\delta^2 F}{\delta a_{\mu i}^* \delta a_{\nu j}} \bigg|_{a_0} \epsilon_{\mu i}^* \epsilon_{\nu j}$$

$$= (2\xi_1 + \xi_2) |\text{Tra}_0 \epsilon^T|^2 + 2\xi_2 \text{Tra}_0^2 \text{Tr} \epsilon^\dagger \epsilon + \xi_{35} \text{Tr} \epsilon^\dagger a_0 \epsilon^T a_0 + \xi_{34} \text{Tra}_0^2 \epsilon^\dagger \epsilon + \xi_{45} \text{Tra}_0^2 \epsilon \epsilon^\dagger$$

$$+ \text{Re}[\xi_1 \text{Tra}_0 a_0^T \text{Tr} \epsilon \epsilon^T + \xi_2 (\text{Tra}_0)^2 + \xi_3 \text{Tra}_0^2 \epsilon \epsilon^T + \xi_4 \text{Tra}_0 \epsilon a_0 + \xi_5 \text{Tra}_0^2 \epsilon^T \epsilon] . \quad (\text{B1})$$

Let us first consider the pure  $A$  stationary state  $a_0(z) = v_0(z) \hat{\mathbf{z}}(\hat{\mathbf{x}} + i\hat{\mathbf{y}})$ . As mentioned in the text, this is also the state of minimum energy within the pure  $A$  family, Eq. (6). This means that Eq. (B1) is positive if  $\epsilon$  is of the pure  $A$  form,  $\epsilon_{\mu i} = \epsilon(z) \hat{\mathbf{z}}_\mu(\hat{\mathbf{x}} + i\hat{\mathbf{y}})_i$ . This allows one to identify a positive definite operator  $L$ ,

$$\langle L \rangle \equiv \langle \epsilon | L | \epsilon \rangle \equiv \int [(-\frac{1}{2} + \xi_{245} v_0^2) |\epsilon|^2 + |\epsilon'|^2] dz > 0 . \quad (\text{B2})$$

For general deviations  $\epsilon_{\mu i}$ , it is straightforward to show that

$$Q = \langle L \rangle_{\epsilon_{z^-}} + \langle 2L \rangle_{\epsilon_{zz}} + (\gamma - 1) \epsilon_{zz}^2 + \langle L + 2\xi_{13} v_0^2 \rangle_{\epsilon_{z^+}} + \langle L \rangle_{\epsilon_{x^-}} + \langle 2L - 2\xi_{45} v_0^2 \rangle_{\epsilon_{xz}}$$

$$+ \langle L + (\xi_3 - \xi_{45}) v_0^2 \rangle_{\epsilon_{x^+}} + \langle L \rangle_{\epsilon_{y^-}} + \langle 2L - 2\xi_{45} v_0^2 \rangle_{\epsilon_{yz}} + (\gamma - 1) \epsilon_{yz}^2 + \langle L + (\xi_3 - \xi_{45}) v_0^2 \rangle_{\epsilon_{y^+}} \quad (\text{B3})$$

where  $\epsilon_{\mu\pm} \equiv \epsilon_{\mu x} \pm i\epsilon_{\mu y}$ . For the  $\xi$ 's tabulated in Table II, it is easy to verify that each term in Eq. (B3) is positive. The pure  $A$  state is therefore locally stable.

Next we consider the  $B$ -planar stationary state  $a_0(z) = h_0 \hat{\mathbf{z}} + g_0(\hat{\mathbf{x}}\hat{\mathbf{x}} + \hat{\mathbf{y}}\hat{\mathbf{y}})$ . To show its local stability, it is useful to decompose  $\epsilon$  in (22) into real and imaginary part,  $\epsilon = r + is$ . Using the fact that  $a_0$  is real and symmetric,  $Q$  can be rewritten as

$$Q = Q_r + Q_s = \int dz \{ -\text{Tr}(rr^T) + \xi_{12} \text{Tra}_0 a_0 \text{Tr}(rr^T) + 2\xi_{12} [\text{Tr}(ra_0)]^2$$

$$+ \xi_{345} [\text{Tr}(a_0 a_0 r r^T) + \text{Tr}(ra_0 r a_0) + \text{Tr}(a_0 a_0 r^T r)] + \gamma r_{\mu z}^2 + r_{\mu x}^2 + r_{\mu y}^2 \}$$

$$+ \int dz \{ -\text{Tr}(ss^T) + (\xi_1 - \xi_2) \text{Tra}_0 a_0 \text{Tr}(ss^T) + 2\xi_{11} [\text{Tr}(sa_0)]^2 + (-\xi_3 + \xi_{45}) \text{Tr}(a_0 a_0 s s^T)$$

$$+ (-\xi_4 + \xi_{53}) \text{Tr}(sa_0 s a_0) + (-\xi_5 + \xi_{34}) \text{Tr}(a_0 a_0 s^T s) + \gamma s_{\mu z}^2 + s_{\mu x}^2 + s_{\mu y}^2 \} . \quad (\text{B4})$$

It is straightforward to show that  $Q_r$  is of the form

$$Q_r = \{r_{xx}, r_{yy}, r_{zz}\} + \{r_{xy}, r_{yx}\} + \{r_{xz}, r_{zx}\} + \{r_{yz}, r_{zy}\} , \quad (\text{B5})$$

where each bracket means terms containing only variables appear inside the bracket. Identical structure holds for  $Q_s$ .

In particular,

$$\{r_{xx}, r_{yy}, r_{zz}\} = \int \{-1 + \xi_{12}(h_0^2 + 2g_0^2)(r_{xx}^2 + r_{yy}^2 + r_{zz}^2) + 2\xi_{12}(r_{xx} + r_{yy})g_0 + r_{zz}h_0\}^2 + 3\xi_{345}[g_0^2(r_{xx}^2 + r_{yy}^2) + r_{zz}^2h_0^2] + \gamma r_{zz}'^2 + r_{zz}''^2 + r_{yy}''^2\}. \quad (\text{B6})$$

Since both  $(h_0, g_0)$  are associated with the state of lowest energy, they are nodeless functions. Thus, without loss of generality, we can use the functions  $\rho_1, \rho_2,$  and  $\rho_3$  defined as  $r_{xx} \equiv g_0\rho_1, r_{yy} \equiv g_0\rho_2, r_{zz} \equiv h_0\rho_3$  in place of the  $r$ 's. Using the stationary condition Eqs. (9) and (10), Eq. (B6) can be rewritten as

$$\{r_{xx}, r_{yy}, r_{zz}\} = \int [2\xi_{345}h_0^4\rho_3^2 + \gamma h_0 h_0''\rho_3^2 + \gamma(h_0\rho_3)^2] + \int [2\xi_{345}g_0^4\rho_1^2 + \gamma h_0^2\rho_3^2 + 2\xi_{345}g_0^4(\rho_1^2 + \rho_2^2) + g_0^2(\rho_1^2 + \rho_2^2)] \quad (\text{B7})$$

which is positive because  $\xi_{345}$  is positive. Following the same procedure, with the definition  $(r_{xy} \equiv g_0\rho_1, r_{yx} \equiv g_0\rho_2), (r_{xz} \equiv h_0\rho_3, r_{zx} \equiv g_0\rho_1), (r_{yz} \equiv h_0\rho_3, r_{zy} \equiv \rho_2)$ , and using Table II, it is straightforward to show that  $\{r_{xy}, r_{yx}\}, \{r_{xz}, r_{zx}\},$  and  $\{r_{yz}, r_{zy}\}$  are positive. Repeating the same procedure to the  $s$  terms, one can show that  $\{s_{xx}, s_{yy}, s_{zz}\}$  and  $\{s_{xy}, s_{yx}\}$  are positive. The perturbations that are harder to show to be stable are  $\{s_{xz}, s_{zx}\}$  and  $\{s_{yz}, s_{zy}\}$ , which have identical structure. In the case of  $\{s_{xz}, s_{zx}\}$ , we have [after defining  $(s_{xz} \equiv h_0\rho_3, s_{zx} \equiv g_0\rho_1)$  and using Eqs. (9) and (10)],

$$\{s_{xz}, s_{zx}\} = \int dz [\rho_3^2(\lambda_3 g_0^2 h_0^2 + \rho_1^2(\lambda_1 g_0^4 + \lambda_1' g_0^2 h_0^2)) + 2\tau h_0^2 g_0^2 \rho_1 \rho_3 + \gamma h_0^2 h_0'' \rho_3^2 + \gamma(h_0\rho_3)^2 + g_0 g_0'' \rho_1^2 + (g_0\rho_1)^2], \quad (\text{B8})$$

where  $\lambda_3 \equiv -\xi_{15} > 0, \lambda_3' \equiv (-4\xi_1 - \xi_3 + \xi_{45}) > 0, \lambda_1 \equiv (-4\xi_1 - 2\xi_5) < 0, \lambda_1' \equiv (-2\xi_1 - \xi_3 + \xi_{45}) < 0,$  and  $\tau \equiv (\xi_3 - \xi_4 + \xi_5) > 0.$  The above inequalities can be seen from Table II. At this point, one notes that  $g_0 > h_0$  (see text). If we replace  $\lambda_3' g_0^2 h_0^2$  and  $\lambda_1' g_0^2 h_0^2$  by the smaller terms  $\lambda_3' h_0^4$  and  $\lambda_1' g_0^4$ , we have

$$\{s_{xz}, s_{zx}\} > \int dz [\rho_3^2(\lambda_3 + \lambda_3')h_0^4 + \rho_1^2(\lambda_1 + \lambda_1')g_0^4 + 2\tau h_0^2 g_0^2 \rho_1 \rho_3 + \gamma(h_0 h_0'' \rho_3^2) + \gamma(h_0\rho_3)^2 + g_0 g_0'' \rho_1^2 + (g_0\rho_1)^2]. \quad (\text{B9})$$

The last four terms are simply  $\gamma(h_0\rho_3')^2 + (g_0\rho_1')^2$ , which is positive. The first four terms turn out to be a positive quadratic form, as it is easy to verify that  $(\lambda_3 + \lambda_3')(\lambda_1 + \lambda_1') > \tau^2$  for all pressures, using Table II. The local stability of this  $B$ -planar state is therefore established.

The instabilities of (6) and (7) for specular boundary condition can be similarly established.

### APPENDIX C: THE EFFECTS OF EXTERNAL SUPERFLOWS AND THE CALCULATION OF SUPERFLUID DENSITIES

Let us first recall the usual scheme of calculating the superfluid density. First one determines the order parameter in the presence of a superflow  $\mathbf{u}$  by minimizing the total free energy  $\int F = \int F_B + \int F_G$  within the class of order parameters of the form  $e^{i2m\mathbf{u}\cdot\mathbf{r}/\hbar} A_{\mu i}$ . The expressions of  $F_B$  and  $F_G$  are given in Eqs. (1) and (2). Let  $A_{\mu i}^0(\mathbf{u})$  be

the equilibrium order parameter for the flow  $\mathbf{u}$ . The superfluid density in the limit of vanishing superflow is defined as

$$(\rho_s)_{ij} = \left. \frac{d^2 f_{\text{total}}(\mathbf{u})}{du_i du_j} \right|_{\mu=0} = \left. \frac{dg_i(\mathbf{u})}{du_j} \right|_{\mu=0}, \quad (\text{C1})$$

where

$$f_{\text{total}}(\mathbf{u}) = \left[ \int F_B(e^{i2m\mathbf{u}\cdot\mathbf{r}/\hbar} A_{\mu i}^0) + \int F_G(e^{i2m\mathbf{u}\cdot\mathbf{r}/\hbar} A_{\mu i}^0) \right] / \text{volume}$$

is the equilibrium free energy density, and  $g_i(\mathbf{u}) \equiv \int p_i [e^{i2m\mathbf{u}\cdot\mathbf{r}/\hbar} A_{\mu i}^0(\mathbf{u})] / \text{volume}$  is the equilibrium current density,

$$p_i [A_{\mu i}] = i(2m/\hbar) A_{\mu j} \frac{\partial F_G}{\partial \nabla_i A_{\mu j}} + \text{c.c.} \quad (\text{C2})$$

For bulk superfluids, where  $A_{\mu i}^{\text{bulk}} = A_{\mu i}^0(\mathbf{u}=0)$ , it is easy to show that the effect of a small flow  $\mathbf{u}$  is to cause a second-order change ( $\sim u^2$ ) in the order parameter,  $A_{\mu i}^0(\mathbf{u}) = [A_{\mu i}^{\text{bulk}} + O(u^2)] e^{i2m\mathbf{u}\cdot\mathbf{r}/\hbar}$ . In very confined geometries, however, the zero flow order parameter  $A_{\mu i}^0(\mathbf{u}=0)$  can have strong spatial variations. A nonvanishing external flow can couple linearly to these spatial variations and cause first-order changes in the order parameter. The general form of this change ( $R$ ) can be represented as

$$A_{\mu i}^0(\mathbf{u}) = [A_{\mu i}^0(\mathbf{u}) + u_j R_{\mu ij} + O(u^2)] e^{i2m\mathbf{u}\cdot\mathbf{r}/\hbar}. \quad (\text{C3})$$

The superfluid density will then be

TABLE II. Table of the  $\beta$  coefficients given in Ref. 9.

$P$ (bar)	$\beta_1$	$\beta_2$	$\beta_3$	$\beta_4$	$\beta_5$
0	-1.000	2.000	2.000	2.000	-2.000
4	-1.011	1.974	1.962	1.934	-2.066
8	-1.023	1.946	1.922	1.868	-2.130
12	-1.034	1.920	1.884	1.802	-2.196
16	-1.041	1.912	1.872	1.772	-2.236
20	-1.048	1.906	1.864	1.746	-2.278
24	-1.056	1.900	1.860	1.728	-2.321
28	-1.062	1.898	1.862	1.714	-2.370

$$(\rho_s)_{ij} = \frac{1}{\text{volume}} \left[ \frac{2m}{\hbar} \right] K \int [(\gamma - 1) A_{\mu i}^0 A_{\mu j}^{*0} + A_{\mu s}^0 A_{\mu s}^{*0} \delta_{ij}] |_{u=0} + T, \quad (\text{C4})$$

where  $T$  represents terms depending on the product  $T(R \nabla A^0) |_{\mu=0}$ . The first term is the conventional expression for superfluid density of bulk superfluids. The second term is caused by the nonvanishing gradients of the zero flow  $A^0$ , which are generic in confined geometries. Although the second term becomes insignificant for large containers, it can be quite substantial for small geometries.

For slab geometries, the  $A$  phase order parameter in the presence of a superflow  $\mathbf{v}_s = u \hat{\mathbf{y}}$  turn out to be, for specular and diffusive cases, respectively,

$$a_{\mu i}^0 = v(\hat{\mathbf{x}} + i\hat{\mathbf{y}})_i, \quad (\text{C5})$$

$$a_{\mu i}^0 = d_\mu (v_1 \hat{\mathbf{x}} + i v_2 \hat{\mathbf{y}} + w \hat{\mathbf{z}})_i, \quad (\text{C6})$$

where  $v$ ,  $v_1$ , and  $v_2$  differ from their zero flow solutions  $v_0$  by quantities of the order of  $u^2$  for small flows. However, the function  $w(z)$  is first order in  $u$ . These results can be derived from the Ginzburg-Landau equation, which is

Eq. (5) with  $a_{\mu i}$  replaced by  $a_{\mu i} e^{i2muy/\hbar}$ , and reads

$$0 = \mathcal{X} - (\gamma - 1)(ik \partial_j a_{\mu j} \delta_{iy} + ik \partial_i a_{\mu y} - k^2 a_{\mu y} \delta_{iy}) - (\partial_j^2 a_{\mu i} + 2ik \partial_y a_{\mu i} - k^2 a_{\mu i}), \quad (\text{C7})$$

where  $\mathcal{X}$  represents Eq. (5) and  $k = 2mu/\hbar$ . When  $k$  is sufficiently small, perturbation theory implies a driving term (for  $i = z$ )  $ik \partial_z a_{\mu y}^0$  in Eq. (C7), which is nonzero (zero) in the diffusive (specular) case. This driving term is the reason for the presence (absence) of the  $w$  term in (C6) and (C5).

We have solved Eq. (C7) numerically as a function of  $u$  and found that the equilibrium states are of the form (C5) and (C6). The superfluid density shown in Fig. 4 is obtained by numerically computing the derivative in Eq. (C1). For cylindrical pores, we find that superflows along the channel only generate  $O(u^2)$  changes in the order parameter.

<sup>1</sup>See for example, A. L. Leggett, Rev. Mod. Phys. **47**, 331 (1975).  
<sup>2</sup>J. P. Pekola, J. T. Simola, P. J. Hakonen, M. Krusius, O. V. Lounasmaa, K. K. Nummila, G. Mamniashvili, R. E. Packard, and G. E. Volovik, Phys. Rev. Lett. **53**, 584 (1984).  
<sup>3</sup>P. Gammel, T. L. Ho, and J. Reppy, Phys. Rev. Lett. **55**, 2708 (1985).  
<sup>4</sup>P. Gammel (private communication); and unpublished.  
<sup>5</sup>M. Freeman and R. C. Richardson (private communication).  
<sup>6</sup>K. Ichikawa, S. Yamasaki, H. Akimoto, T. Kodama, T. Shigi, and H. Kojima, Phys. Rev. Lett. **55**, 1949 (1987).

<sup>7</sup>V. Ambegaokar, P. G. deGennes, and D. Rainer, Phys. Rev. A **9**, 2676 (1974).  
<sup>8</sup>E. Thuneberg, Phys. Rev. B **33**, 5124 (1986).  
<sup>9</sup>K. Bedell (private communication).  
<sup>10</sup>F. Fishman and I. A. Privorotskii, J. Low Temp. Phys. **25**, 225 (1976).  
<sup>11</sup>P. Muzikar, J. Phys. (Paris) Colloq. **39**, C6-53 (1978).  
<sup>12</sup>E. Thuneberg (unpublished).  
<sup>13</sup>S. L. Alder and T. Piran, Rev. Mod. Phys. **56**, 1 (1984).